AFRL-RZ-WP-TP-2012-0132

SUPERCONDUCTING PROPERTIES OF $(M_x/YBa_2Cu_3O_{7-\delta y})_N$ MULTILAYER FILMS WITH VARIABLE LAYER THICKNESS $_x$ (POSTPRINT)

T.J. Haugan, P.N. Barnes, T.A. Campbell, N.A. Pierce, M.F. Locke, I. Brockman, A.L. Westerfield, J.M. Evans, R. Morgan, P. Klenk, B.C. Harrison, and A.D. Chaney

Mechanical Energy Conversion Branch
Energy/Power/Thermal Division

F.J. Baca

Los Alamos National Laboratory

I. Maartense

University of Dayton Research Institute

FEBRUARY 2012

AIR FORCE RESEARCH LABORATORY
PROPULSION DIRECTORATE
WRIGHT-PATTERSON AIR FORCE BASE, OH 45433-7251
AIR FORCE MATERIEL COMMAND
UNITED STATES AIR FORCE

REPORT DOCUMENTATION PAGE

Form Approved
OMB No. 0704-0188

1. REPORT DATE *(DD-MM-YY)*	2. REPORT TYPE	3. DATES COVERED *(From - To)*
February 2012	Journal Article Postprint	04 April 2005 – 04 April 2007

4. TITLE AND SUBTITLE

SUPERCONDUCTING PROPERTIES OF $(M_x/YBa_2Cu_3O_{7-\delta y})_N$ MULTILAYER FILMS WITH VARIABLE LAYER THICKNESS $_x$ (POSTPRINT)

5a. CONTRACT NUMBER
In-house

5b. GRANT NUMBER

5c. PROGRAM ELEMENT NUMBER
62203F

6. AUTHOR(S)

T.J. Haugan, P.N. Barnes, T.A. Campbell, N.A. Pierce, M.F. Locke, I. Brockman, A.L. Westerfield, J.M. Evans, R. Morgan, P. Klenk, B.C. Harrison, and A.D. Chaney (AFRL/RZPG)
F.J. Baca (Los Alamos National Laboratory)
I. Maartense (University of Dayton Research Institute)

5d. PROJECT NUMBER
3145

5e. TASK NUMBER
32

5f. WORK UNIT NUMBER
314532ZE

7. PERFORMING ORGANIZATION NAME(S) AND ADDRESS(ES)

Mechanical Energy Conversion Branch (AFRL/RZPG)
Energy/Power/Thermal Division
Air Force Research Laboratory, Propulsion Directorate
Wright-Patterson Air Force Base, OH 45433-7251
Air Force Materiel Command, United States Air Force

Los Alamos National Laboratory
Los Alamos, NM 87545

University of Dayton Research Institute
Dayton, OH 45469

8. PERFORMING ORGANIZATION REPORT NUMBER
AFRL-RZ-WP-TP-2012-0132

9. SPONSORING/MONITORING AGENCY NAME(S) AND ADDRESS(ES)

Air Force Research Laboratory
Propulsion Directorate
Wright-Patterson Air Force Base, OH 45433-7251
Air Force Materiel Command
United States Air Force

10. SPONSORING/MONITORING AGENCY ACRONYM(S)
AFRL/RZPG

11. SPONSORING/MONITORING AGENCY REPORT NUMBER(S)
AFRL-RZ-WP-TP-2012-0132

12. DISTRIBUTION/AVAILABILITY STATEMENT

Approved for public release; distribution unlimited.

13. SUPPLEMENTARY NOTES

Journal article published in the *Journal of Electronic Materials*, Vol. 36, No. 10, 2007. © 2007 TMS. The U.S. Government is joint author of the work and has the right to use, modify, reproduce, release, perform, display, or disclose the work.

PA Case Number: 88ABW-2007-0627; Clearance Date: 04 Apr 2007. Work on this effort was completed in 2007. Paper has color content.

14. ABSTRACT

The superconducting properties of $(M_x/YBa_2Cu_3O_{7-dy})_N$ multilayer films were studied for varying layer thickness x. Different M phases were examined including green-phase Y_2BaCuO_5 (211), Y_2O_3, $BaZrO_3$, CeO_2, $SmBa_2Cu_3O_{7-d}$ (Sm123), brown-phase La_2BaCuO_5 (La211), and MgO. Multilayer $(M_x/YBa_2Cu_3O_{7-dy})_N$ structures were grown by pulsed laser deposition onto $SrTiO_3$ or $LaAlO_3$ single-crystal substrates by alternate ablation of separate $YBa_2Cu_3O_{7-d}$ (123) and M targets, at temperatures of 750 °C to 790 °C. The x layer thickness was varied from 0.1 nm to 4.5 nm, and the y 123 layer thickness was kept constant within a given range of 10 to 25 nm. Different M phase and x layer thicknesses caused large variations of the microstructural and superconducting properties, including superconducting transition (T_c), critical current density as a function of applied magnetic field $J_c(H)$, self-field J_c(77 K), and nanoparticle layer coverage. Strong flux-pinning enhancement up to 1 to 3x was observed to occur for M additions of 211 and $BaZrO_3$ at 65 to 77 K, Y_2O_3 at 65 K, and CeO_2 for H < 0.5 T. $BaZrO_3$ had a noticeably different epitaxy forming smaller size nanoparticles ~8 nm with 3 to 4*x* higher areal surface particle densities than other M phases, reaching 5×10^{11} nanoparticles cm^{-2}. To optimize flux pinning and J_c (65 to 77 K, H = 2 to 3 T), the M layer thickness had to be reduced below a critical value that correlated with a nanoparticle surface coverage <15% by area. Unusual effects were observed for poor pinning materials including Sm123 and La211, where properties such as self-field J_c unexpectedly increased with increasing *x* layer thickness.

15. SUBJECT TERMS

superconducting properties, microstructural, applied magnetic field, flux-pinning, nanoparticle, epitaxy, pulsed laser deposition

16. SECURITY CLASSIFICATION OF:			17. LIMITATION OF ABSTRACT:	18. NUMBER OF PAGES	19a. NAME OF RESPONSIBLE PERSON (Monitor)
a. REPORT	b. ABSTRACT	c. THIS PAGE			Timothy J. Haugan
Unclassified	Unclassified	Unclassified	SAR	16	19b. TELEPHONE NUMBER *(Include Area Code)* N/A

Journal of ELECTRONIC MATERIALS, Vol. 36, No. 10, 2007
DOI: 10.1007/s11664-007-0229-y

Superconducting Properties of $(M_x/YBa_2Cu_3O_{7-\delta y})_N$ Multilayer Films with Variable Layer Thickness *x*

T.J. HAUGAN,[1,3] P.N. BARNES,[1] T.A. CAMPBELL,[1] N.A. PIERCE,[1] F.J. BACA,[1] M.F. LOCKE,[1] I. BROCKMAN,[1] A.L. WESTERFIELD,[1] J.M. EVANS,[1] R. MORGAN,[1] P. KLENK,[1] B.C. HARRISON,[1] A.D. CHANEY,[1] and I. MAARTENSE[2]

1.—Air Force Research Laboratory, Propulsion Directorate – Power Division, Wright-Patterson AFB, OH 45433-7251, USA. 2.—University of Dayton Research, AFRL/MLPSE, Wright-Patterson AFB, OH 45433-7707, USA. 3.—e-mail: timothy.haugan@wpafb.af.mil

The superconducting properties of $(M_x/YBa_2Cu_3O_{7-\delta y})_N$ multilayer films were studied for varying layer thickness *x*. Different M phases were examined including green-phase Y_2BaCuO_5 (211), Y_2O_3, $BaZrO_3$, CeO_2, $SmBa_2Cu_3O_{7-\delta}$ (Sm123), brown-phase La_2BaCuO_5 (La211), and MgO. Multilayer $(M_x/YBa_2Cu_3O_{7-\delta y})_N$ structures were grown by pulsed laser deposition onto $SrTiO_3$ or $LaAlO_3$ single-crystal substrates by alternate ablation of separate $YBa_2Cu_3O_{7-\delta}$ (123) and M targets, at temperatures of 750°C to 790°C. The *x* layer thickness was varied from 0.1 nm to 4.5 nm, and the *y* 123 layer thickness was kept constant within a given range of 10 to 25 nm. Different M phase and *x* layer thicknesses caused large variations of the microstructural and superconducting properties, including superconducting transition (T_c), critical current density as a function of applied magnetic field $J_c(H)$, self-field J_c(77 K), and nanoparticle layer coverage. Strong flux-pinning enhancement up to 1 to 3*x* was observed to occur for M additions of 211 and $BaZrO_3$ at 65 to 77 K, Y_2O_3 at 65 K, and CeO_2 for $H < 0.5$ T. $BaZrO_3$ had a noticeably different epitaxy forming smaller size nanoparticles ~8 nm with 3 to 4*x* higher areal surface particle densities than other M phases, reaching 5×10^{11} nanoparticles cm^{-2}. To optimize flux pinning and J_c (65 to 77 K, $H = 2$ to 3 T), the M layer thickness had to be reduced below a critical value that correlated with a nanoparticle surface coverage <15% by area. Unusual effects were observed for poor pinning materials including Sm123 and La211, where properties such as self-field J_c unexpectedly increased with increasing *x* layer thickness.

Key words: Superconductor, thin film, $YBa_2Cu_3O_{7-\delta}$, multilayer, nanoparticle, flux pinning, critical current density, magnetic field, pulsed laser deposition

INTRODUCTION

The development of high-temperature superconductor $YBa_2Cu_3O_{7-\delta}$ (YBCO or 123) thin films on polycrystalline substrates (coated conductors) with $J_c > 1$ MA/cm^2 offers great promise for incorporation into power applications such as generators or motors operating at 77 K.[1–5] YBCO has excellent properties at 77 K including high $J_c(H)$ due to strong flux pinning. However it is of interest to increase $J_c(H)$ even further, to increase wire performance and reduce production costs almost proportionally.[1,2] For type-II superconductors, it is known that flux pinning can be increased by incorporating a high density of extended nonsuperconducting defects into the material.[2–4] The defect size should be approach the coherence length ~2–4 nm at 4.2 to 77 K to maximize pinning.[2–4]

(Received January 19, 2007; accepted May 17, 2007; published online September 14, 2007)

Many methods of introducing defects can be considered to increase flux pinning in YBCO,[2–4] and recent efforts have studied the use of $(M_x/123_y)_N$ heterostructures to introduce ~3 to 20 nm-size island-growth nanoparticles or even larger-diameter plate-like defects into the films.[5–17] A number of different second-phase additions M have been tested, including M = green-phase 211,[5–12] Y_2O_3,[11,12,14,15] CeO_2,[11–13] $IrZrO_3$,[16] $BaZrO_3$,[17] and other phases with negative effects on T_c and/or $J_c(H)$ including M = La211,[11,12] MgO,[11,12] and Sm123.[12] Studies of $(M_x/123_y)_N$ heterostructures can provide basic information about the relative pinning properties of different M phases, and specific parameters of flux pinning such as the effects of different layer spacings.

While initial results have been presented on the effect of different pinning-layer thickness x in $(M_x/123_y)_N$ structures, detailed studies have not yet been published.[5–17] This paper presents a systematic comparison of film properties for selected M phases and different x layer thickness. A significant result observed is that the surface coverage is an important constant factor to optimize flux pinning, regardless of the M phase. Significant differences in T_c, self-field J_c ($J_{c\text{-self-field}}$) and $J_c(H)$ were also observed, varying with the M phase, which are not yet fully understood. In this study, the 123 thickness y was held constant in the range of about 10 to 25 nm, as the superconducting properties did not change dramatically for constant x and this range of y. Therefore y was constant in the studies herein to allow the detailed study of the change of the x layer thickness.

The M phase additions studied are shown in Table I, which also includes the lattice mismatch with respect to 123. As studied preliminarily previously and shown in more detail herein, the lattice mismatch of M to 123 is an important factor that strongly affects pinning and the magnitude of $J_c(H)$ achieved.[11,12]

Only high lattice-mismatched materials, >4% with respect to 123, increased J_c(77 K, $H > 0.5$ T) for the parameter ranges tested: 123 layer thickness y = 10 to 25 nm, and heater temperature = 775 to 790°C, as shown herein and studied previously.[11,12] Interestingly phase additions with very close lattice mismatching of <1% dramatically lowered J_c(77 K, $H > 0.5$ T) by a factor of 10 to 100, suggesting that the density and type of pinning defects are consistently reduced by inducing more-perfect growth.[11,12] Additional evidence is also presented herein on how the chemical reactivity can negatively affect superconducting properties.[11,12]

EXPERIMENTAL

Multilayer $(M_x/123_y)_N$ films were deposited by pulsed laser deposition (PLD), using the parameters and conditions described in detail previously.[5–14,17,18] Deposition parameters were 248 nm laser wavelength, ~3.2 J/cm^2 laser fluence, 25 nm pulse length, 2 to 4 Hz laser repetition rate, 5.5 cm target-to-substrate distance, 83 to 92% dense targets, 300 mTorr oxygen partial pressure, and a postdeposition anneal at 500°C in 1 atm of oxygen.[18] The heater block temperature varied slightly for the different M phases studied: 775°C for 211, Y_2O_3, La211, Sm123 and MgO, 790°C for $BaZrO_3$,[17] and 750°C for CeO_2 to avoid the formation of large precipitates that are observed with a higher growth temperature of 775°C to 785°C,[11–13] unless

Table I. Crystal Properties of M Phases Studied, and the Lattice Mismatch to 123. The Lattice Parameters of Epitaxy Are $\bar{a} = (a,b)_{avg}$, $a'' = a/2$, $a^* = a/\sqrt{2}$

Material	Lattice Type	Lattice Parameters (nm)	Lattice Parameter of Epitaxy (nm)	Lattice Mismatch to 123 $\bar{a}$ (%)
$YBa_2Cu_3O_{7-\delta}$	Orthorhombic	a = 0.3825 b = 0.3886 c = 1.166	$\bar{a}$ = 0.3855	
$SmBa_2Cu_3O_{7-\delta}$	Orthorhombic	a = 0.3855 b = 0.3899 c = 1.1721	$\bar{a}$ = 0.3877	+0.57
CeO_2	Cubic	a = 0.54115	a^* = 0.3827	–0.75
Y_2O_3	Cubic	a = 1.0604	$a^{*\prime\prime}$ = 0.3749	–2.8
Y_2BaCuO_5	Orthorhombic	a = 0.7132 b = 1.218	a'' = 0.3566	–7.5**
		c = 0.5659	c'' = 0.2830	–27.6**
$BaZrO_3$	Cubic	a = 0.41898	a' = 0.41898	+8.7
MgO	Cubic	a = 0.4203	a' = 0.4203	+9.0
La_2BaCuO_5	Tetragonal	a = 0.67015 c = 0.58211	a'' = 0.3351	–13.1**

**Epitaxy of Y_2BaCuO_5 onto 123 is b-axis oriented[6], so the lattice misfit is calculated for both a'' and c''.

otherwise noted. These differences of heater block temperature can cause small variations of J_c and T_c, but were sufficiently close to allow an initial study for comparison. The substrates used were $LaAlO_3$ (LAO) and $SrTiO_3$ (STO) 100 oriented single crystals, with epi-polish. For multilayer films, an automated target rotation and pulse-triggering system was used to control the deposition sequences, with a period of about 13 s, during which the deposition was stopped and different targets were rotated into position. The deposition rate for each pinning material was calibrated prior to multilayer deposition. In this paper, the term 'pseudolayer' is used to describe the M phase layer. The pseudolayer thickness in the multilayer films was calculated assuming smooth continuous film coverage, although the insulating layer in most cases consisted of discontinuous and discrete nanoparticles. Deposition rates for 123 were 13 to 15 nm/min and for M phases varied from 10 nm/min to 20 nm/min for all phases except MgO, which was 3 nm/min and $BaZrO_3$ and La211, which were 30 to 35 nm/min. To obtain lower M deposition rates than usual for M = CeO_2, Y_2O_3 and $BaZrO_3$, an attenuating lens was added to reduce the laser fluence by ~30%. The total film thickness was kept in the range of 0.25 to 0.35 μm to provide consistent comparisons. The film thickness of every sample was measured multiple times across acid-etched step edges with a profilometer (KLA-Tencor, P15), to obtain the average value and standard error of measurement <5%.

The superconducting transition temperature (T_c) was measured using an alternating current (AC) susceptibility technique with the amplitude of the magnetic sensing field strength, h varying from 0.025 Oe to 2.2 Oe, at a frequency of approximately 4 Hz. Note that the AC susceptibility provides information about the primary and secondary transitions of the entire film, rather than a defined path that is obtained with transport T_c measurements. Transition widths of T_c were defined as the full-width at half-maximum (FWHM) of the χ'' transition measured for a 2.2 Oe field. Magnetic J_c measurements were made with a vibrating sample magnetometer (VSM) at magnetic field strengths of 0 to 9 T, and a ramp rate of 0.01 T s^{-1}. The J_c of the square samples was estimated using a simplified Bean model $J_c = 15\Delta M/R$, where M = magnetization/volume from M–H loops, and R = radius of volume interaction = square side, for consistency.[18] Characterization of the microstructures was performed with scanning electron microscopy in ultra-high-resolution mode (SEM, FEI–Sirion). Transport J_c measurements were made with microbridges that were 0.03 to 0.05 cm wide by 0.3 cm long using the four-point contact method, and with a voltage criteria of 1 μV/cm. Microbridges were made by 248 nm UV laser etching through alumina masks with a laser fluence 0.1 J/cm^2, a laser pulse length 25 ns, at 1 Hz. The critical current was measured in liquid nitrogen at 77.2 K. Current was applied to the sample by a step-ramp method: a current step interval of 0.2 to 0.5 s, a ramp rate of 0.25 to 1.0 A/s, and a voltage sample period two to four times smaller than the current step interval. The maximum current step size was 0.1 A.

RESULTS AND DISCUSSION

The effect of varying the M phase on T_c transitions is shown in Fig. 1, as a function of x, the pseudolayer thickness. As shown in Fig. 1, M-phase nanolayer addition generally lowered the T_c onset on average by about 1 K for 211, BZO, Y_2O_3, La211 and Sm123, and even more (by about 2 to 4 K) for CeO_2 and MgO. As the surface pseudolayer thickness increased above a critical value, T_c started to decrease approximately linearly for both Y_2O_3[14] and 211. The critical value for decrease of T_c for both 211 and Y_2O_3 did not correlate with pseudolayer thickness, but rather correlated closely with nanoparticle surface layer coverage >20%, as will be shown later. The T_c FWHM of the M phases also varied considerably. The T_c FWHMs were large by about 6 to 8 K for MgO and La211 for even very low pseudolayer thickness <0.2 nm, and the full χ'' T_c transitions were not completed above 77 K for these materials, as shown in Fig. 1 for a pseudolayer thickness of x ~0.5 nm, and also given previously for x ~1 nm.[11] These wide transitions suggest that the materials were degraded by chemical reaction and diffusion into the superconductor. $BaZrO_3$ had the narrowest T_c FWHM transitions of about 1.4 K for a moderate layer thickness, constant for a wide range of pseudolayer thickness. This was followed by 211, Y_2O_3 and Sm123 with T_c FWHM ~1.5 to 3 K. As the T_c FWHM widened above 3 K for 211 and Y_2O_3, the T_c transition correlated roughly to a decrease of the self-field J_c, as shown in Fig. 1. The reason for the correlation is being studied presently.[19]

The variation of self-field J_c is also shown in Fig. 1, for a range of pseudolayer thicknesses. The trends of self-field J_c in Fig. 1 correlated roughly with the trends measured for T_c and T_c FWHM. Different M phase additions with low T_c and/or wide T_c FWHM including MgO, CeO_2, and La211 and Y_2O_3 for $x > 1.3$ nm had low $J_{ct} \leq 1$ MA/cm^2 for the range of pseudolayer coverages considered. La211 had an increase of $J_{c\text{-self-field}}$ as the pseudolayer thickness increased, which was correlated with a slight increase of T_c and decrease of T_c FWHM. For CeO_2 the self-field J_c dependence on pseudolayer thickness was flat, similar to the T_c. Sm123 had a slight upward trend of self-field J_c with increasing pseudolayer thickness, which was consistent with the increase of T_c and no change of T_c FWHM.

The microstructural properties of $(M_x/123_y)_N$ film surfaces are shown in Figs. 2–4, imaged by SEM at high magnifications of 100,000 times for M addition = 211, MgO, $BaZrO_3$, Sm123, and also a reference 123-only film. Similar micrographs for M = Y_2O_3, CeO_2, and La211 additions at the same

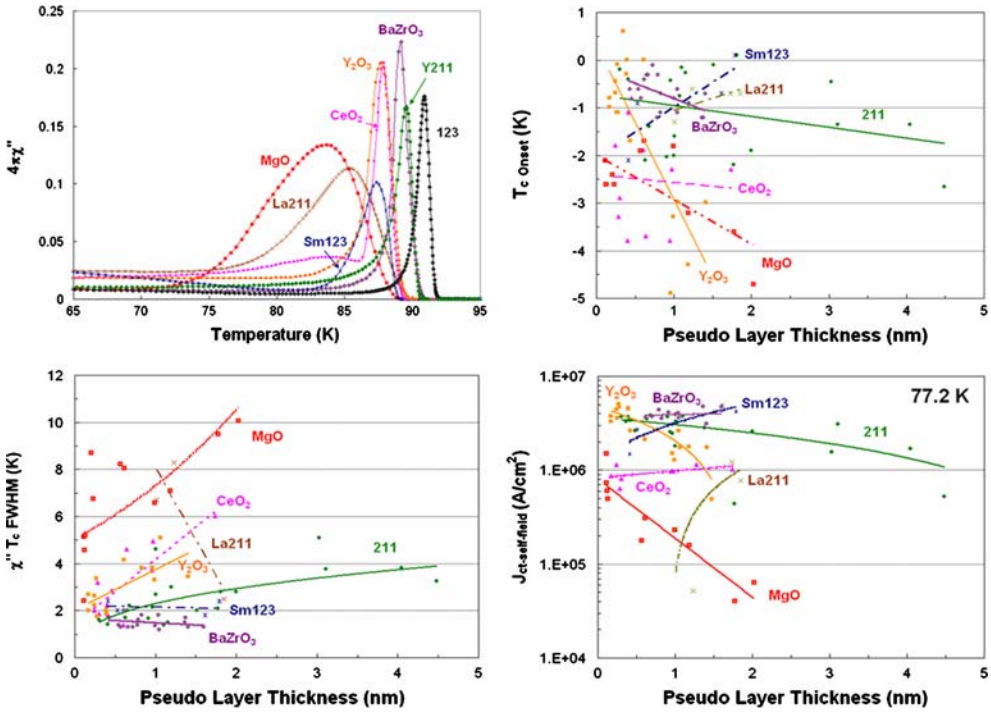

Fig. 1. T_c measurements by AC susceptibility χ'' at 2.2 Oe and self-field J_{ct} measurements of $(M_x/123_y)_N$ films for varying pseudolayer thickness: (upper left) T_c transitions for x ~0.5 nm; (upper right) relative T_c onset compared to 123 average; (lower left) T_c FWHM measurements, (lower right) self-field J_{ct} at 77.2 K. Lines are guides to the eye.

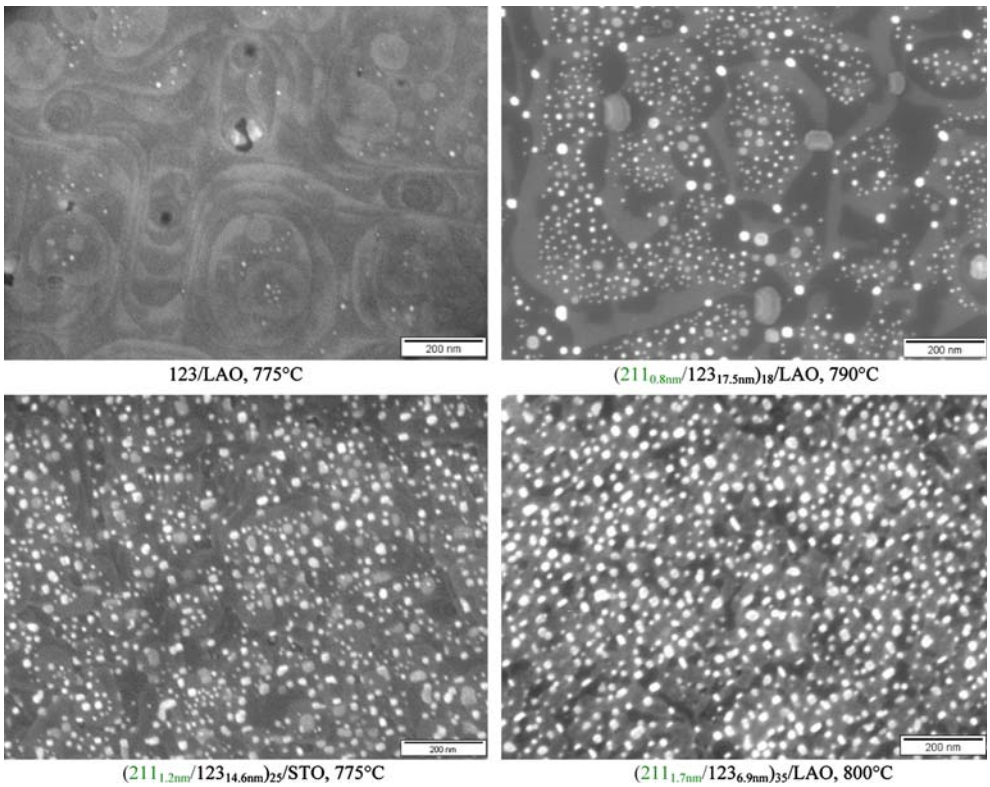

Fig. 2. SEM micrographs of a 123-only film and $(211_x/123_y)_N$ multilayer films.

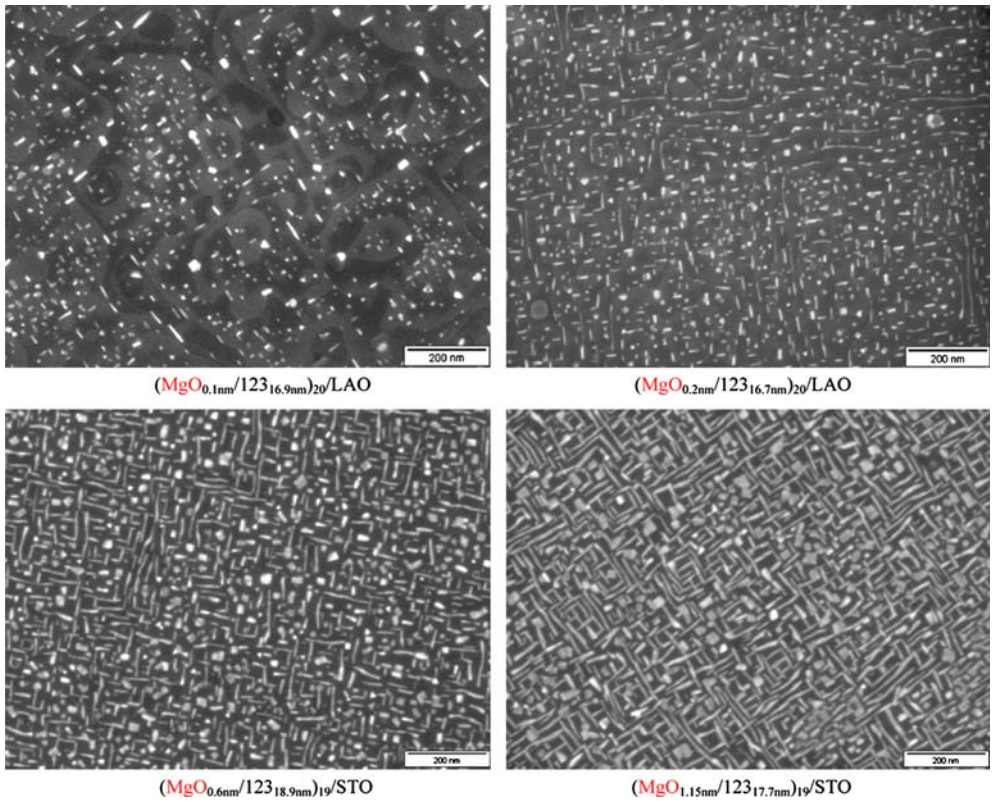

$(MgO_{0.1nm}/123_{16.9nm})_{20}/LAO$ $(MgO_{0.2nm}/123_{16.7nm})_{20}/LAO$

$(MgO_{0.6nm}/123_{18.9nm})_{19}/STO$ $(MgO_{1.15nm}/123_{17.7nm})_{19}/STO$

Fig. 3. SEM micrographs of $(MgO_x/123_{\sim 18\ nm})_N$ multilayer films.

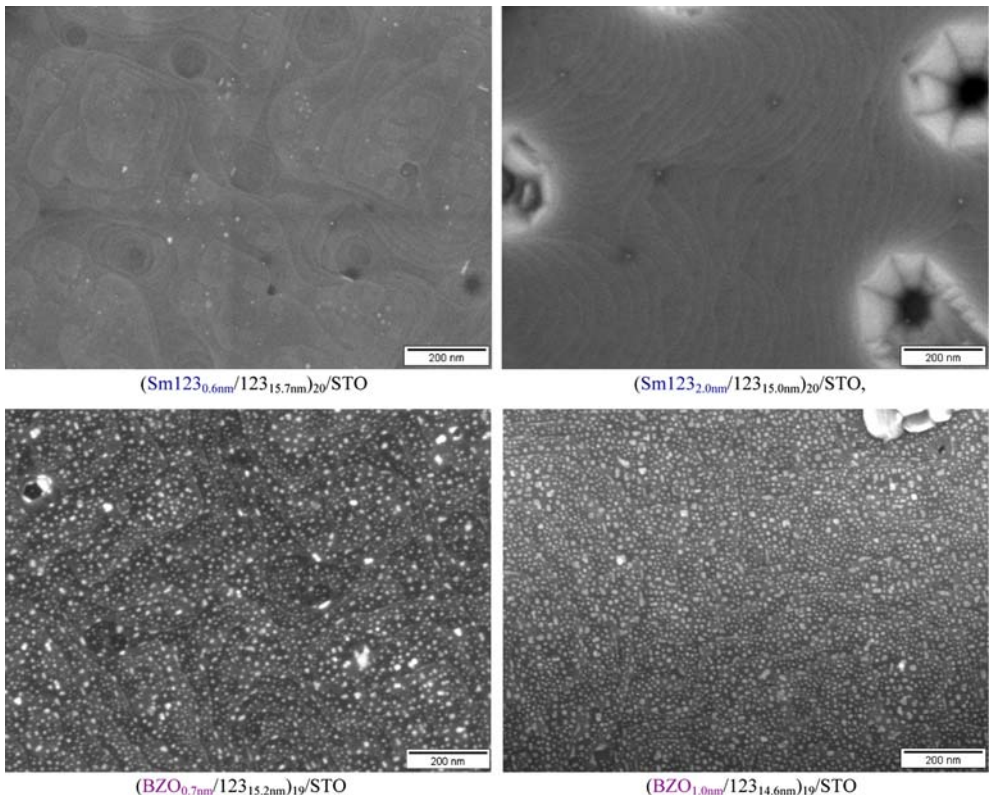

$(Sm123_{0.6nm}/123_{15.7nm})_{20}/STO$ $(Sm123_{2.0nm}/123_{15.0nm})_{20}/STO,$

$(BZO_{0.7nm}/123_{15.2nm})_{19}/STO$ $(BZO_{1.0nm}/123_{14.6nm})_{19}/STO$

Fig. 4. SEM micrographs of $(Sm123_x/123_{\sim 15nm})_N$ and $(BaZrO_{3x}/123_{\sim 15\ nm})_N$ multilayer films.

magnification were published previously,[11,13,14] and micrographs for $BaZrO_3$ were shown at higher magnification.[17] La211 addition did not produce any visible nanoparticle formations.[11] The micrographs in Figs. 2–4 show a noticeable variation of nanoparticle sizes, densities and shapes for different M phase additions. Note that the nanoparticles appear white or lighter due to enhanced surface charging and emission of imaging electrons, which suggests that they are insulating. Additions of M = Y_2O_3 and 211 had similar size (9 to 13 nm) and areal surface densities 0.8 to 1.4×10^{11} nanoparticles cm^{-2}.[6,14] However the surface coverage of Y_2O_3 was about two times higher for similar pseudolayer thickness, which will be shown in more detail later. Phase M = Y_2O_3,[14] 211 and MgO had incomplete surface coverage with gaps of 50–100 nm for low specific M layer thickness, which was not observed for M = $BaZrO_3$ except for much smaller scale of about 10 nm.

Nanolayer addition M = $BaZrO_3$ had markedly different nanoparticle coverage than other M phases, achieving both much higher areal surface densities of up to 5×10^{11} nanoparticles cm^{-2} and smaller average nanoparticle size <8 nm (Fig. 4). Presumably M = $BaZrO_3$ would provide more-consistent and stronger pinning properties, but this has not yet been confirmed for $J_c(H//c\text{-axis})$.[17] However $J_c(H/ab\text{-plane})$ properties were markedly three times higher for M = BZO compared to other pinning materials.[17] Nanoparticle formations for MgO were noticeably different from other M phases, forming nanorod structures. The M = MgO nanorod structures were quite different from M = $BaZrO_3$ disc-shaped nanoparticles, and since MgO and BZO have almost the same lattice mismatch of ~9% and cubic crystal structure (Table I), the formation of nanorods for MgO nanolayers suggests that a different noncubic crystal structure has formed possibly from reaction with 123. Reaction of Mg and 123 lowers T_c strongly by about 15 K for very small substitution $x = 0.025$ in $YBa_{2-x}Mg_xCu_3O_{7-\delta}$ (<0.5 at.%), and Mg was found to substitute mostly on the Cu site and/or react with Ba to form oxides.[20–22] We speculate that the nanorods in Fig. 3 could be a-axis-oriented distorted-orthorhombic $YBa_2Cu_{3-x}Mg_xO_{7-\delta}$,[20] double-perovskite $(Y,Mg)_2Ba_2O_6$,[23] (Cu,Mg)O with $x \leq 0.2$,[24] or other Mg-reacted phase such as distorted-cubic $Ba(Cu,Mg)O_{2-\delta}$.

While the microstructures of $(MgO/123)_N$ films are interesting, with potentially different pinning properties that might result from the rod structures, the T_c and $J_{c\text{-self-field}}$ are reduced so much that such advantages probably cannot be realized. It should also be noted that $(MgO/123)_N$ films appear to have disrupted the formation of the 123 island structures that were observed in other $(M/123)_N$ multilayer films to some degree. Therefore $(MgO/123)_N$ interlayers might be useful to level or homogenize the films in more-complex or thicker multilayer structures. Finally the microstructural properties of $(Sm123/123)_N$ multilayer films are interestingly different for Sm123 $x = 0.6$ nm compared to Sm123 $x = 2$ nm. The Sm123 $x = 2.0$ films had higher T_c and $J_{c\text{-self-field}}$ compared to Sm123 $x = 0.6$ films, which may correlate to the larger grain structure in Fig. 4. The reason why the Sm123 $x = 0.6$ nm film had worse J_c is speculated to be caused by disruption of pinning defects such as dislocation networks or planar defects, as discussed previously for CeO_2.[11–13] The formation of large pore defects was also observed for Sm123 $x = 2.0$ films.

Properties of nanoparticle formations including surface coverage, areal surface densities, average size, and expected height are plotted in Fig. 5 for different M phase additions. The trends observed in SEM micrographs in Figs. 2–4 were measured quantitatively and represented in Fig. 5. The most notably unique nanoparticle formations observed were for $BaZrO_3$ with 3–5x higher nanoparticle areal densities achieved than other phases; e.g. up to 5×10^{11} nanoparticles cm^{-2}. This high nanoparticle density is equivalent to a ~11 T matching field, and much higher than the 2 to 3 T matching field for other phase additions. $BaZrO_3$ also had the smallest average nanoparticle size among all phases studied, ~8 nm for variable pseudolayer thickness. The nanoparticle surface coverage for all materials changed as expected by increasing nearly linearly with increasing pseudolayer thickness. The trend for MgO was slightly different; e.g., slightly decreasing from linearity with increasing pseudolayer thickness, which can be explained by increasing nanoparticle height or incomplete chemical reaction of MgO and 123, which reduces the relative amount of material forming nanoparticles. The variation of average nanoparticle size (surface diameter) is also plotted in Fig. 5, which shows gradual growth except for MgO which had two to three times faster growth than other phases. By looking at the combined graphs in Fig. 5, epitaxial growth of Y_2O_3, 211, and MgO occurred primarily by increasing the areal density of nanoparticles, as well as slowly increasing the nanoparticle size and height, whereas $BaZrO_3$ grew initially by increasing strongly in nanoparticle density. After reaching a critical level of pseudolayer thickness, the nanoparticle areal number density for all phases decreased as expected as the nanoparticles joined together to form complete layers, as shown. The expected nanoparticle height was calculated simply from the area coverage and pseudolayer thickness, and plotted in Fig. 5. The ratio of measured/expected nanoparticle heights gives a measure of the deposition efficiency of the M phase; ξ = measured/expected nanoparticle height. While these ratios were not measured at this time, we suspect for MgO the ratio of ξ to be greater than 1 if it is reacting with 123 as expected. Also we believe the ratio of ξ for 211 might be as low as 0.3 to 0.5, as 211 may be difficult to deposit directly as a second-phase, and the formation of Y_2O_3 and 123

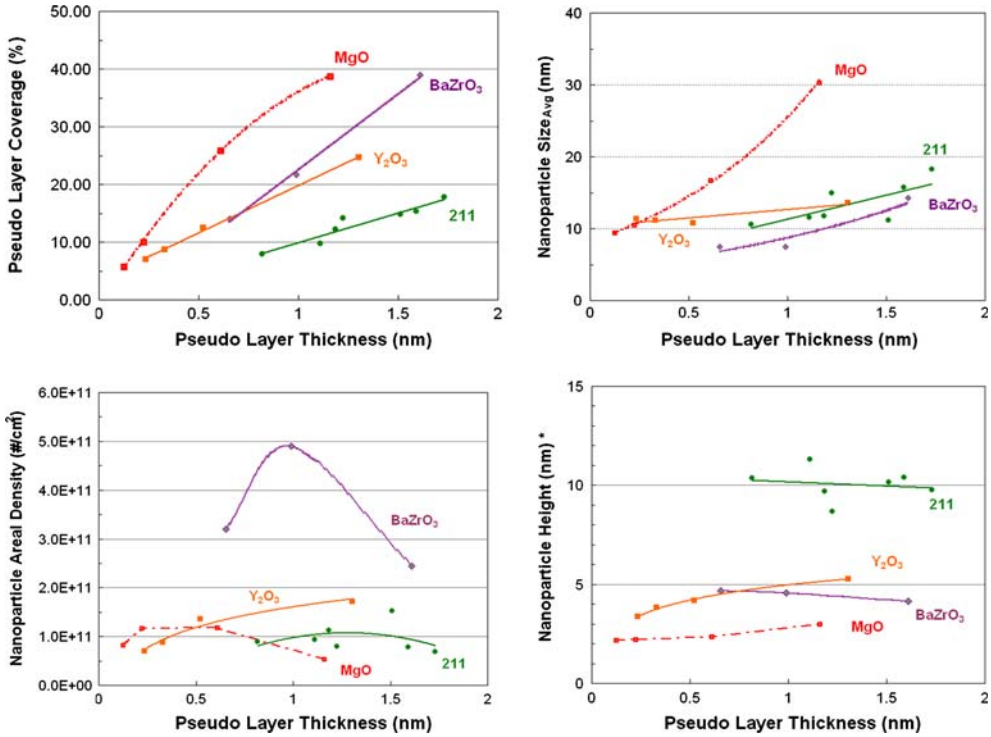

Fig. 5. Properties of nanoparticle formations on $(M_x/123_y)_N$ film surfaces. The nanoparticle size is the average diameter assuming disc-shaped particles. The data plotted is measured except for nanoparticle heights which are predicted values assuming 100% deposition efficiency of the M phases. Lines are guides to the eye.

film by-products may be occurring to some degree. Nanoparticle heights of 211 expected in Fig. 5 were very consistently ~10 nm, which is quite high considering the particles themselves barely have this average diameter. However 211 nanoparticle heights by TEM cross-sections of 211 pseudolayers were typically less than 5 nm on average,[6,12] which suggests that the prediction of $\xi < 1$ is correct.

The effect of M phase additions on $J_c(H$, 65 to 77 K) was measured by magnetic methods in Fig. 6 for complete $J_c(H)$ curves for a pseudolayer coverage of x ~0.5 nm, and for selected values of H = 2 to 3 T and variable pseudolayer thickness x. The trends of $J_c(H)$ in Fig. 6 correlate roughly with the trends observed for T_c and self-field J_c: MgO, CeO_2 and La211 additions generally had the lowest values of $J_c(H)$. MgO, which had the widest T_c FWHM transitions and the clearest evidence of chemical reaction, had the lowest $J_c(H)$ of all the phases studied. Sm123 had remarkably similar J_c(77 K, $H > 0.5$ T) properties to CeO_2 for flux pinning, despite the larger differences in the T_c FWHM and self-field J_c. The lattice mismatches for CeO_2 and Sm123 were both <1% with respect to 123, which we believe indicates that lattice mismatch is an important variable to control microstructural defects that affect flux pinning, rather than the electrical properties of the phases.[11,12] At 77 K, only M = 211 and $BaZrO_3$ showed evidence of increased pinning, while M = Y_2O_3 had almost exactly the same flux pinning as 123-only films. At 65 K the properties were different however, with M = 211, $BaZrO_3$ and Y_2O_3 all having strong increases of $J_c(H)$ up to three times, and $BaZrO_3$ having slightly better $J_c(H = 3$ T) properties for $x < 0.7$ nm. Interestingly M = CeO_2 addition showed a unique increase of J_c at low fields $H < 0.5$ T at both 65 K and 77 K, despite large decrease of J_c at higher fields $H > 0.5$ T. Also for $H < 0.5$ T CeO_2 was different from Sm123. Further work is necessary to understand these differences and what types of defects causes these varying effects. Also, unusually for M = La211 and x ~1.5 nm, the $J_c(H)$ values increased to be almost equal to other M phases and 123. Since nanoparticles were not formed with La211 addition,[11,12] this suggests that other microstructural defects are effective for flux pinning at H = 2 to 3 T with a large addition of La211 phase (~9% by volume). These combined results indicate that different defects are forming with varying M addition, causing varying properties of $J_c(H)$. Some defects formed pins well at low field $H < 0.5$ T while others pin at high fields $H > 0.5$ T. Nanoparticles including 211 pin well at both low and high fields, however are possibly not the best at low fields $H < 0.5$ T, as shown herein for different pseudolayer thicknesses and previously for selected pseudolayer thicknesses.[11–13]

While Fig. 6 plots $J_c(H)$ properties for varying pseudolayer thickness, it is also of interest to replot the same curves as a function of nanoparticle surface layer coverage, as shown in Fig. 7. As shown there, the surface layer coverage is closely

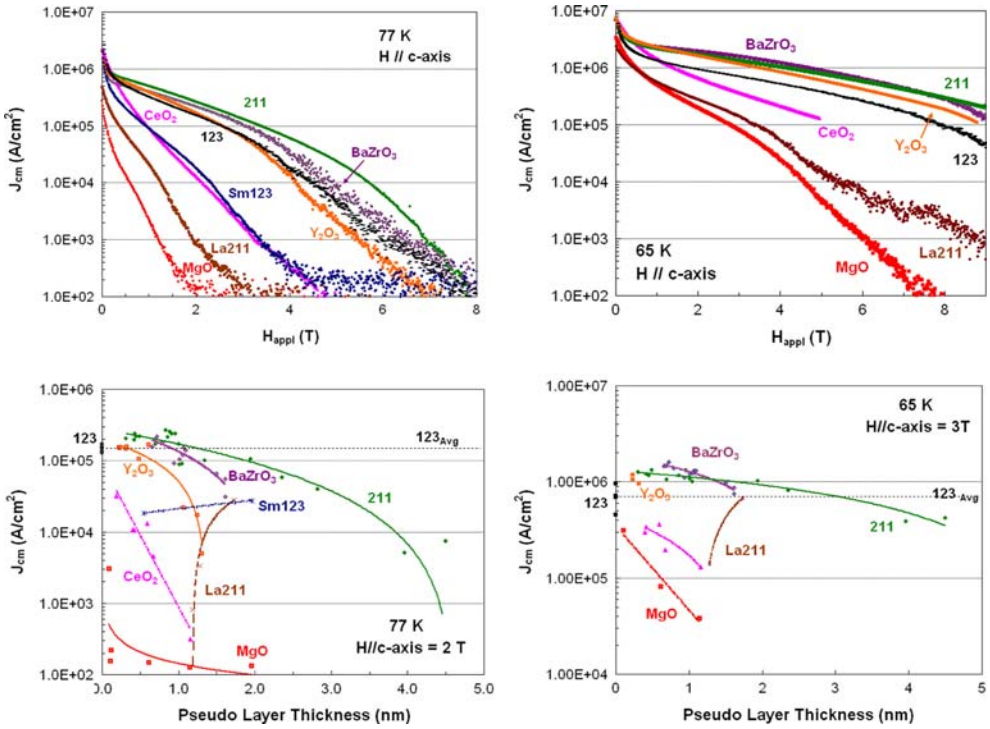

Fig. 6. Critical current density measured by magnetic methods for varying M phase addition: (upper) for approximate constant pseudolayer thickness x ~0.5 nm; (lower) variable pseudolayer thickness and constant magnetic field. Lines are guides to the eye.

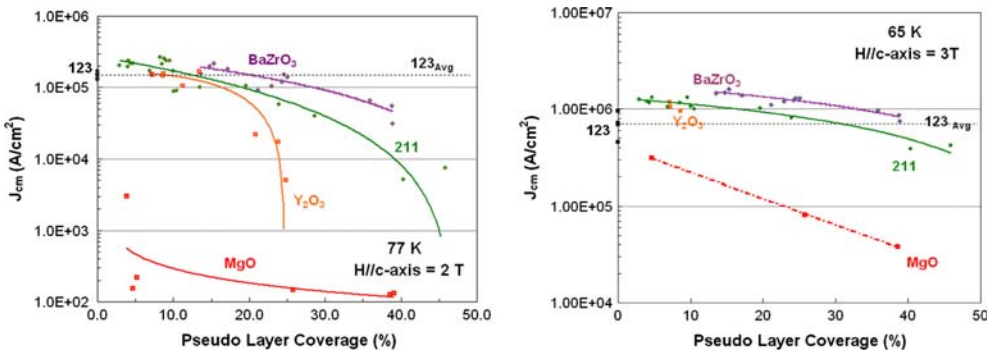

Fig. 7. Critical current density using the same data points from Fig. 6, plotted as a function of pseudolayer coverage rather than pseudolayer thickness. The curve fits from Fig. 5 (top left) were used to convert pseudolayer thickness to pseudolayer coverage. Lines are guides to the eye.

correlated to flux pinning regardless of the M phase, which indicates that it is an important experimental parameter to control and optimize for every pinning material. The slight difference for $BaZrO_3$ compared to Y_2O_3 and 211 might be explained by different nanoparticle coverage, as discussed previously. Figure 7 indicates that the two-dimensional (2-D) surface layer coverage must be reduced to <15 to 20% to increase $J_c(H)$ of $(M/123)_N$ films to comparable or higher values than 123-only films, for all three nonreactive phases studied: M = 211, Y_2O_3 and $BaZrO_3$. If the 2-D pseudolayer coverage is > 20%, J_c begins to drop significantly below the average for 123 films. Interestingly this 2-D layer coverage percentage is roughly similar to theoretical predictions of the maximum for flux pinning that occurs with ~15 vol.% defect addition, calculated using classical models of three-dimensional (3-D) current flow.[25] For magnetic field penetration in YBCO with $H//c$-axis, circulating currents must flow in the ab-plane to form vortices, so similar considerations might apply for 2-D compared to 3-D modeling. However it is unknown yet whether there is a connection between these considerations. It should be noted that these conclusions were reached by imaging nanoparticles on film surfaces, and slightly different shifts of the $J_c(H)$ versus pseudolayer coverage curves and interpretations might result from imaging nanoparticles on the inside layers of the films. On the inside layers, nanoparticles might be slightly smaller, have higher number density, and be shorter in height, as the M layers

have only about 13 s to rest before the next 123 superconducting layer is deposited. However despite these possible differences, the plots for $J_c(H)$ versus surface coverage in Fig. 7 are consistent, indicating that surface layer coverage is an important variable to control.

CONCLUSIONS

The properties of $(M_x/123_y)_N$ multilayer films were studied for varying M pseudolayer thickness x. Strong flux pinning was observed for M = 211, $BaZrO_3$, and Y_2O_3 that varied with applied field and temperature, and for CeO_2 for $H < 0.5$ T. $BaZrO_3$ had a notably different epitaxy forming smaller size nanoparticles ~8 nm and three to four times greater areal surface particle densities than other M phases, reaching 5×10^{11} nanoparticles cm^{-2}. To optimize flux pinning, the M layer thickness had to be reduced below a critical value that correlated with surface layer coverage <15% by area. This interestingly correlates closely with theoretical predictions of a maximum of flux pinning occurring for ~15% defect volume additions, however the explanation of this comparing 2-D vortex current flow to 3-D current flow[25] is only speculation so far. Unusual effects were observed for poor pinning materials including Sm123 and La211, where properties such as self-field J_c unexpectedly increased with increasing M layer thickness. The effects of M-phase lattice mismatch and probable chemical reactions between M phases and 123 on flux pinning were further presented herein.[11,12]

ACKNOWLEDGEMENTS

The authors would like to express appreciation to Lyle Brunke, John Murphy, Joe Kell, and David Blubaugh for assistance with $J_c(H,T,\theta)$ and film thickness measurements. The authors are also grateful for support of this work by the U.S. Air Force Office of Scientific Research and the Air Force Research Laboratory—Propulsion Directorate.

REFERENCES

1. P.N. Barnes, M.D. Sumption, and G.L. Rhoads, *Cryogenics* 45, 670 (2005).
2. D. Larbalestier, A. Gurevich, D.M. Feldmann, and A. Polyanskii, *Nature* 414, 368 (2001).
3. T. Matsushita, *Supercond. Sci. Technol.* 13, 730 (2000).
4. M. Murakami, D.T. Shaw and S. Jin, *Processing and Properties of High T_c Superconductors Volume 1*, *Bulk Materials*, ed. S. Jin (New Jersey: World Scientific Publishing Co. Pte. Ltd., 1993). .
5. T. Haugan, P.N. Barnes, I. Maartense, E.J. Lee, M. Sumption, and C.B. Cobb, *J. Mat. Res.* 18, 2618 (2003).
6. T. Haugan, P.N. Barnes, R. Wheeler, F. Meisenkothen, and M. Sumption, *Nature* 430, 867 (2004).
7. T. Haugan, P. Barnes, R. Nekkanti, J.M. Evans, L. Brunke, I. Maartense, J.P. Murphy, A. Goyal, A. Gapud, and L. Heatherly, *Epitaxial Growth of Functional Oxides*, ed. A. Goyal (Proceedings of the Electrochemical Society, Ed., 2005).
8. T.J. Haugan, P.N. Barnes, T.A. Campbell, A. Goyal, A. Gapud, L. Heatherly, and S. Kang, *Physica C* 425, 21 (2005).
9. P.N. Barnes, T.J. Haugan, M.D. Sumption, S. Sathiraju, J.M. Evans, and J.C. Tolliver, *Trans. MRS-J* 29(4), 1385 (2004).
10. P.N. Barnes, T.J. Haugan, M.D. Sumption, and B.C. Harrison, *IEEE Trans. Appl. Supercond.* 15, 3766 (2005).
11. T.J. Haugan, P.N. Barnes, T.A. Campbell, J.M. Evans, J.W. Kell, L.B. Brunke, J.P. Murphy, C. Varanasi, I. Maartense, W. Wong-Ng, and L.P. Cook, *IEEE Trans. Appl. Supercond.* 15, 3770 (2005).
12. T.J. Haugan, *In-situ Approach to Introduce Flux pinning in YBCO* (Studies of High Temperatures Superconductors, Book Series), ed. M. Parathaman, V. Selvamanickam (NY: Nova Sci., 2006, submitted for publication).
13. P.N. Barnes, T.J. Haugan, C.V. Varanasi, and T.A. Campbell, *Appl. Phys. Lett.* 85, 4088 (2004).
14. T.A. Campbell, T.J. Haugan, P.N. Barnes, I. Maartense, J. Murphy, and L. Brunke, *Physica C* 423, 1 (2005).
15. A.A. Gapud, D. Kumar, S.K. Viswanathan, C. Cantoni, M. Varela, J. Abiade, S.J. Pennycook, and D.K. Christen, *Supercond. Sci. Technol.* 18, 1502 (2005).
16. J. Hänisch, C. Cai, R. Hühne, L. Schultz, and B. Holzapfel, *Appl. Phys. Lett.* 86, 122508 (2005).
17. T. Haugan, P.N. Barnes, T.A. Campbell, N.A. Pierce, F.J. Baca, and I. Maartense. *IEEE Trans Appl Supercond*, 17, 3724 (2007).
18. T. Haugan, P.N. Barnes, L. Brunke, I. Maartense, and J. Murphy, *Physica C* 297, 47 (2003).
19. P. Barnes, I. Maartense, T.L. Peterson, T.J. Haugan, A.L. Westerfield, L.B. Brunke, S. Sathiraju, and J.C. Tolliver, *Correlation of AC Loss Data from Magnetic Susceptibility Measurements with YBCO Film Quality* (MRS Proceedings, EXS–3, pp. EE6.4.1–3, 2004).
20. T. Komatsu, H. Meguro, R. Sato, O. Tanaka, K. Matusita, and T. Yamashita, *J. Appl. Phys.* 27, L2063 (1988).
21. H. Koinuma, K. Fukuda, T. Hashimoto, and K. Fueki, *J. Appl. Phys.* 27, L1216 (1988).
22. J.M.S. Skakle, *Mat. Sci. Eng.* R23, 1 (1998).
23. R. Weinstein and R.-P. Sawh, *Physica C* 383, 438 (2003).
24. J. Assal, B. Hallstedt, and L.J. Gauckler, *Z. Metallkd.* 87, 568 (1997).
25. A. Gurevich, Florida State Univ., private communication and presented at Stanford-Wisconsin Workshop on Coated Conductors, April 24–26, 2006.